

Steady-State and Pre-Steady-State Kinetic Evaluation of Severe Acute Respiratory Syndrome Coronavirus (SARS-CoV) 3CL^{pro} Cysteine Protease: Development of an Ion-Pair Model for Catalysis

James Solowiej, James A. Thomson, Kevin Ryan, Chun Luo,[‡] Mingying He, Jihong Lou, and Brion W. Murray*

Pfizer Global Research and Development, La Jolla, Pfizer Inc., 10777 Science Center Drive, San Diego, California 92121

Received October 18, 2007; Revised Manuscript Received December 19, 2007

ABSTRACT: Severe acute respiratory syndrome (SARS) was a worldwide epidemic caused by a coronavirus that has a cysteine protease (3CL^{pro}) essential to its life cycle. Steady-state and pre-steady-state kinetic methods were used with highly active 3CL^{pro} to characterize the reaction mechanism. We show that 3CL^{pro} has mechanistic features common and disparate to the archetypical proteases papain and chymotrypsin. The kinetic mechanism for 3CL^{pro}-mediated ester hydrolysis, including the individual rate constants, is consistent with a simple double displacement mechanism. The pre-steady-state burst rate was independent of ester substrate concentration indicating a high commitment to catalysis. When homologous peptidic amide and ester substrates were compared, a series of interesting observations emerged. Despite a 2000-fold difference in nonenzymatic reactivity, highly related amide and ester substrates were found to have similar kinetic parameters in both the steady-state and pre-steady-state. Steady-state solvent isotope effect (SIE) studies showed an inverse SIE for the amide but not ester substrates. Evaluation of the SIE in the pre-steady-state revealed normal SIEs for both amide and ester burst rates. Proton inventory (PI) studies on amide peptide hydrolysis were consistent with two proton-transfer reactions in the transition state while the ester data was consistent with a single proton-transfer reaction. Finally, the pH-inactivation profile of 3CL^{pro} with iodoacetamide is indicative of an ion-pair mechanism. Taken together, the data are consistent with a 3CL^{pro} mechanism that utilizes an “electrostatic” trigger to initiate the acylation reaction, a cysteine–histidine catalytic dyad ion pair, an enzyme-facilitated release of P₁, and a general base-catalyzed deacylation reaction.

Severe acute respiratory syndrome (SARS)¹ was a worldwide epidemic that appeared in November of 2002. The overall mortality rate was estimated by the World Health Organization to have reached 15% of all patients and up to 50% for patients over 65 years of age. In the wake of significant media attention, the research community applied intense and productive attention to this new viral disease. Four months after the first SARS case was identified, a new coronavirus was shown to be the causative agent: SARS-CoV (1). Within 1 month, the entire genome of SARS-CoV had been sequenced (2, 3). The SARS-CoV was shown to

be phylogenetically distinct from the three previously identified coronavirus groups (4). The main protease responsible for maturation of the polyproteins and central to the life-cycle was identified as a cysteine protease similar to the 3C family of cysteine proteases: 3CL^{pro} (also known as M^{pro}). The 3CL^{pro} has been cloned, expressed in *Escherichia coli*, and purified (5, 6). Its enzymatic activity has been measured by the development of both discontinuous and continuous enzymatic assays (6–11). Initial kinetic studies showed that the 3CL^{pro} had modest activity (k_{cat}/K_m of $177 \text{ M}^{-1} \text{ s}^{-1}$) (6), while other reports had high protease activity ($k_{\text{cat}}/K_m > 10000 \text{ M}^{-1} \text{ s}^{-1}$) (8, 12). Differences in enzymatic activity and dimerization constants may be attributed to the 3CL^{pro} construct design, the substrate, or the handling/storage conditions (11, 13).

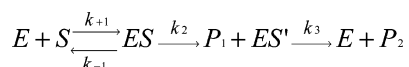
The crystal structure of the protease has been released (PDB entry 1q2w by Bonnano et al. 2003) with other structures published subsequently (14, 15). 3CL^{pro} has been characterized as having a chymotrypsin-fold (14, 16). The structure revealed that the full-length protease contains a catalytic domain (aa1–184), a linker region (aa185–200), and a putative regulatory domain (aa201–303). Structural studies have provided some insight into the 3CL^{pro} reaction mechanism. The active protease is a homodimer with the Cys145–His41 catalytic dyad located in the cleft between the first two domains (7, 14–16). Detailed studies of the

* To whom correspondence should be addressed. Tel: 858-622-6038. Fax: 858-526-4240. E-mail: brion.murray@pfizer.com.

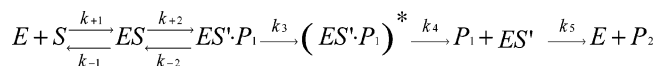
[‡] Present address: Accelagen, 11585 Sorrento Valley Road, Suite 107, San Diego, CA 92121.

¹ Abbreviations: SARS, severe acute respiratory syndrome; SARS-CoV, severe acute respiratory syndrome coronavirus; 3CL^{pro}, 3C-like protease; D₂O, deuterium oxide; SIE, solvent isotope effect; PI, proton inventory; HEPES, 4-(2-hydroxyethyl)piperazine-1-ethanesulfonic acid; BTP, bis-tris propane, 1,3-bis[tris(hydroxymethyl)methylamino]propane; MES, 2-morpholinoethanesulfonic acid; DTT, dithiothreitol; pNA, *p*-nitroaniline; pNP, *p*-nitrophenol; FRET, fluorescence resonance energy transfer; ITC, isothermal titration calorimetry; EDTA, ethylenediaminetetraacetic acid; DMSO, dimethylsulfoxide; Dabcyl, [4-(4-dimethylaminophenylazo)benzoic acid]; IA, iodoacetamide; Tamra, 5-carboxytetramethylrhodamine; Edans, 5-[2'-(aminoethyl)amino]-naphthalenesulfonic acid; IPTG, isopropyl- β -thiogalactopyranoside; PCR, polymerase chain reaction; TFA, trifluoroacetic acid; RFU, relative fluorescence units.

Scheme 1



Scheme 2



functions of the individual domains have revealed that the carboxy-terminal domain (aa201–303) has a critical role in the formation of the active dimer (17).

While at least eight superfamilies of cysteine proteases exist, our understanding of cysteine protease mechanism is derived primarily from studies of the papain family of cysteine proteases or inferred from related serine proteases (18). Papain is the prototypical cysteine protease, which catalyzes peptide hydrolysis with a catalytic dyad ion pair (Cys25–His159), which is oriented by a third residue (Asn175) (18). For the acylation reaction of papain, the ion-pair dyad is the catalytic device responsible for the nucleophilic attack on the substrate's scissile amide carbonyl, and it also is involved in the facilitation of the leaving group stabilization (18–21). For papain, His159 acts as a general base to facilitate the activation of an active site water in the deacylation half-reaction (19). With 3CL^{pro}, an analogous catalytic dyad (Cys145–His41) has been observed in the crystal structure. But unlike papain, the histidine residue of the 3CL^{pro} catalytic dyad is oriented by a water molecule not an asparagine residue (16). The other common enzymatic mechanism for proteolytic peptide cleavage is general base catalysis. The fundamental feature of a general base mechanism is that the catalytic group participates in a proton-transfer that stabilizes the transition state. General base catalysis is the commonly accepted mechanism for chymotrypsin (22). Chymotrypsin has a catalytic triad (Ser195/His57/Asp102) that acts as a charge relay system to increase the nucleophilicity of Ser195 through the abstraction of the hydroxyl proton in a concerted attack of the substrate carbonyl of the scissile bond.

The minimal model for cysteine protease catalysis (Scheme 1) is a three-step reaction that first involves the binding of the substrate to form a Michaelis complex (ES). Next, an acylation reaction occurs with the simultaneous formation of the covalent enzyme acyl intermediate (ES') and the alcohol or amine product (P₁). Finally, a deacylation reaction occurs through the hydrolysis of the ES' acyl intermediate to generate the second product, P₂. In this model, the acylation rate is described by *k*₂ and the deacylation rate by *k*₃. An alternative model (five step) has been proposed that has an additional conformational change to facilitate the release of P₁ (Scheme 2) (23). The (ES'·P₁)^{*} complex represents the enzyme conformation from which the alcohol or amine P₁ rapidly diffuses to leave (ES').

The enzymatic mechanism for 3CL^{pro} has been proposed to utilize chymotrypsin-like general base catalysis and not a papain-like thiolate–imidazolium ion-pair mechanism (10). To support this assignment, the authors presented multiple lines of evidence. They showed that the mutation of the catalytic cysteine to serine (C145S) was active with a 40-fold reduction of activity. An inverse solvent isotope effect (SIE) was observed for the wild-type 3CL^{pro}, while a normal

SIE was observed for the C145S mutant. Last, the measured p*K*_a values were reported to be consistent with a general base mechanism. This first reported kinetic study used a 3CL^{pro} construct that had an additional N-terminal residue, which significantly reduced enzymatic activity.

In this paper, we have further studied the mechanism of the 3CL^{pro} protease using steady-state and pre-steady-state methods on amide and ester substrate hydrolysis reactions. The rate constants that define the kinetic mechanism of ester hydrolysis were characterized. Included in this report are solvent isotope effect and proton inventory studies utilizing amide and ester substrates. Although proton inventory studies have been widely used for serine proteases, they have not been widely used with cysteine proteases (20). The proton inventory studies coupled with pre-steady-state isotope effect evaluation provide a deeper level of understanding of the recently discovered cysteine protease 3CL^{pro}. We also used the mechanistic approach for characterizing the catalytic mechanism of a cysteine protease: pH dependence of iodoacetamide inactivation. The inactivation profile is more consistent with an ion-pair mechanism. Taken as a whole, our data are more consistent with the 3CL^{pro} catalysis of the acylation reaction occurring through an ion-pair mechanism and the catalysis of the deacylation reaction by a general base mechanism. Evidence is provided for an “electrostatic switch” to trigger the acylation reaction and an enzyme-facilitated release of the first product.

MATERIALS AND METHODS

Materials. Peptide 1, peptide 2, and peptide 3 were purchased from SynPep (Dublin, CA) and had the following purities: >97%, >93%, and >91%, respectively. Peptide 4, peptide 5, and peptide 6 were purchased from CPC Scientific (San Jose, CA) and had the following purities: >95%, >93%, and >90.1%, respectively. The following reagents were purchased from Sigma-Aldrich Chemical Co. (St Louis, Mo): HEPES, BTP bis-tris propane, MES, DTT, DMSO, EDTA, D₂O, iodoacetamide, pNA, and pNP. Tween-20 was purchased from Calbiochem (San Diego, CA).

Expression of 3CL^{pro}. The design of the 3CL^{pro} was based on the genome sequence of the Urbani strain SARS-CoV coronavirus (GenBank accession number AY278741, nucleotides 9985–10902), and the synthesis of the 3CL^{pro} DNA was prepared by Blue Heron Biotechnology (Bothell, WA). With the resulting DNA as a template, the gene encoding the mature form of 3CL^{pro} (residues 1–306) was amplified by PCR with forward primer 5'-GTGCTCATGAGTG-GTTTTAGGAAAATGGCATTCCCGTCA-3' and reverse primer 5'-AAGCTTATTGGAAGGTAACACCAGAGCAT-TGTCTAAC-3'. The PCR products were cloned into pCR-Blunt II TOPO vector (Invitrogen, Carlsbad, CA). The 3CL^{pro} DNA was excised from the TOPO vector and subcloned into the *Nco*I and *Hind*III sites of the pET28a vector (Novagen, Madison, WI). The resulting expression construct encoded the mature form of the 3CL^{pro} (residues 1–306) with the addition of the initiation codon. The correct sequences were confirmed by DNA sequencing of both strands. 3CL^{pro} with the deletion of C-terminal two residues (residues 1–304) was made by substituting reverse primer 5'-AAGCTTAG-GTAACACCAGAGCATTGTCTAACACATC-3' for PCR amplification. The expression constructs were transformed

into *E. coli* BL21(DE3) (Invitrogen). A single colony of the transformant was grown at 37 °C to an OD₆₀₀ of 0.7 and then transferred to 23 °C. The cells continued to grow to OD₆₀₀ = 1.0. The expression was induced for 6 h with 0.4 mM IPTG. The cells were harvested by centrifugation using JLA 8.1000 rotor in Beckman Avanti J-20 XP centrifuge at 9400g and stored at -80 °C.

Purification of 3CL^{pro}. A cell pellet was thawed briefly at room temperature and resuspended in 25 mM Tris (pH 8.0), 50 mM NaCl, 0.1 mM EDTA, and 5 mM DTT. Subsequent steps were carried at 4 °C. Cells were lysed by microfluidization and cleared by ultracentrifugation (Beckman L8-M) at 125171 × *g* for 45 min. The cleared lysate was loaded onto a 10 mL Q-sepharose high-performance column (Amersham, Piscataway, NJ). 3CL^{pro} was collected in the flow-through and loaded to a 10 mL phenyl sepharose high-performance column (Amersham) after adjusting the salt concentration to 0.6 M (NH₄)₂SO₄ and 0.5 M NaCl and pH to 7.5. The column was washed with 15–30 column volumes of 25 mM Tris-HCl, pH 7.5, 0.5 M NaCl, 0.6 M (NH₄)₂SO₄, 0.1 mM EDTA, and 5 mM DTT. 3CL^{pro} was eluted with a 15-column-volume linear gradient to 25 mM Tris, pH 7.5, and 5 mM DTT. Fractions containing 3CL^{pro} were identified by SDS-PAGE, pooled, and dialyzed overnight against 25 mM Tris-HCl, pH 7.5, 100 mM NaCl, 0.1 mM EDTA, and 5 mM DTT. Concentrated 3CL^{pro} was loaded onto a HiPrep 26/60 Sephacryl 200 column (Amersham) equilibrated in the dialysis buffer, and eluted in the same buffer. 3CL^{pro} was pooled, concentrated to 10–20 mg/mL, flash frozen, and stored at -80 °C. Protein concentration was measured spectrophotometrically using calculated molar extinction coefficient of 32590 M⁻¹ cm⁻¹. Micromass Q-TOF microanalysis gave a single mass peak at 33844 Da, in agreement with the calculated mass of 33845 Da for the mature 3CL^{pro}, indicating that the initiation methionine was completely removed.

Isothermal Titration Calorimetry (ITC). Isothermal titration calorimetry experiments were performed using a VP-ITC titration microcalorimeter from Microcal LLC (Northampton, MA). The syringe was filled with a solution containing 186.5 μM 3CL^{pro}, and the cell was filled with a solution containing 10 μM inhibitor. Both samples were in 20 mM HEPES (pH 7.0), 1.0 mM EDTA, 0.005% Tween 20 with 4% DMSO added and were degassed immediately prior to use. The protein had been exhaustively dialyzed against 20 mM HEPES (pH 7.0), 1.0 mM EDTA, 0.005% Tween 20 at 4 °C. The inhibitor solution was prepared by diluting a 10 mM stock solution in 100% DMSO with the protein dialysate. The final DMSO concentration was 4%. To minimize the heats of dilution, 4% DMSO was added to the dialyzed protein solution. The titrations were performed at 25 °C. Ten minutes after a preliminary 2 μL injection a series of twelve 10 μL injections spaced 60 min apart were performed. In order to make appropriate corrections for heats of dilution, a machine blank (buffer into buffer), a macromolecule dilution control (protein into buffer), and a ligand dilution control (buffer into inhibitor) were performed. After correction for the heats of dilution, the data were fit using the ORIGIN software package provided with the instrument. The data were fit using a simple one-set-of-sites model. Because the binding was irreversible, only the fitted stoichiometry was reported.

3CL^{pro} HPLC Assay. The 3CL^{pro} HPLC assay measured the protease-catalyzed cleavage of unlabeled peptides (peptides 1 and 2). Proteolytic activity of 3CL^{pro} was measured over 5 min at 25 °C in a 50 μL reaction containing 200 nM 3CL^{pro}, 20 mM HEPES (pH 7.5), 1 mM EDTA, 200 μM substrate, 1.2% DMSO, 0.005% Tween-20, and 2 mM DTT. The reaction was terminated with the addition of 200 μL of acetonitrile/TFA/water (10%/0.1%/89.9%). The peptide absorbances (215 nm) were analyzed by reverse-phase HPLC (HP 1100 HPLC system) on a Zorbax SB-C8 column (2.1 mm × 50 mm, Agilent). Peptides were resolved using a 20 min 10–95% linear gradient of acetonitrile in 0.1% TFA. For example, peptide 1 (SITSAVLQSGFRKMA) was cleaved to SITSAVLQ and SGFRKMA. Both products were isolated and characterized by mass spectrometry to confirm their identity. Chemically synthesized peptide products were used as standards.

3CL^{pro} FRET Assay. For enhanced sensitivity and continuous monitoring of the proteolytic activity of 3CL^{pro}, continuous fluorescence resonance energy transfer (FRET) assays were developed based on peptides 3 and 4. The 3CL^{pro} FRET assay measures the protease-catalyzed cleavage of peptide 3 Tamra-SITSAVLQSGFRKMAK-(DabcyI)-OH to Tamra-SITSAVLQ and SGFRKMAK-(DabcyI)-OH. Initial rates were measured by following the fluorescence of the cleaved Tamra (ex 558 nm, em 581 nm) peptide using a Tecan Safire fluorescence plate reader at room temperature over the course of 10 min. Typical reaction solutions contained 20 mM HEPES (pH 7.0), 1 mM EDTA, 4.0 μM FRET substrate, 4% DMSO, 0.005% Tween-20, and 2 mM DTT. A typical signal was 32000 RFU with a background of 7400 RFU. Assays were initiated with the addition of 25 nM 3CL^{pro}. The extent of the reaction was determined by producing a standard curve with chemically synthesized peptide fragments (SynPep Dublin, CA). The experiments were performed under first-order kinetics by maintaining 3CL^{pro} substrate turnover at <10%. A second FRET substrate, peptide 4 was used to characterize proteolytic activity of 3CL^{pro} (ex 355 nm, em 558 nm). Typical reaction solutions were the same as above with the Tamra-DabcyI substrate with the exception of the buffer where 20 mM BTP (pH 7.0) was substituted for HEPES. A standard curve with the pair of chemically synthesized Tamra- and DabcyI-labeled cleavage products (Pfizer, La Jolla) was generated to determine the amount of SARS-3CL^{pro}-mediated turnover in a typical FRET assay. The amount of cleavage was determined to be under 10%. We evaluated the enzymatic activity as a function of enzyme concentration with 20 μM peptide 3 and found a linear relationship (*R* = 0.998) between 10 and 300 nM, indicating that the assay accurately measured product formation. Pseudo-first-order conditions (4 μM peptide 3, 200 nM 3CL^{pro}) were used to assess the substrate specificity (*k*_{cat}/*K*_m) for peptide 3. Under pseudo-first-order conditions, the first-order rate constant (*k*) that describes the full progress curve when divided by the enzyme concentration will yield the *k*_{cat}/*K*_m value. For peptide 3, the first-order rate constant *k* = 0.00280 ± 0.00002 s⁻¹ obtained with 200 nM 3CL^{pro} yielded a *k*_{cat}/*K*_m value of 14000 ± 88 M⁻¹ s⁻¹.

3CL^{pro} Colorimetric Assays. The colorimetric assay amide substrate, peptide 5, SITSAVLQ-pNA, was used to further characterize the proteolytic activity of 3CL^{pro}. A typical reaction of 0.2 mL contained 12 mM BTP (pH 7.0), 4%

DMSO, 2 mM DTT, and 0.005% Tween-20. The absorbance produced by the cleavage of pNA (400 nm) was measured in cuvettes using a Beckman DU650 spectrophotometer at room temperature over the course of 10 min. The amount of pNA released was calculated using the molar absorptivity. This molar absorptivity of pNA was determined to be 13200 M⁻¹ cm⁻¹ under our experimental conditions using analytical grade pNA. To ensure that experiments were performed under first-order conditions, 3CL^{pro} substrate turnover was determined to be <10%.

The colorimetric assay substrate SITS AVLQ-pNP (peptide 6) was used to characterize the enzymatic activity of 3CL^{pro} with an ester substrate. Typical reaction solutions contained 20 mM HEPES (pH 7.0), 4% DMSO, and 0.005% Tween-20. The absorbance produced by the cleavage of pNP (400 nm) was measured using a Beckman DU650 spectrophotometer at room temperature over the course of 10 min. The amount of pNP released was calculated using the molar absorptivity 7160 M⁻¹ cm⁻¹ determined under our experimental conditions using spectrophotometric grade pNP. 3CL^{pro} substrate turnover was determined to be <10% to ensure the experiments were performed under first-order conditions.

Pre-Steady-State Analysis. Pre-steady-state experiments were performed on an Applied Photophysics SX.18MV-R stopped flow spectrophotometer fitted with a 20 µL cell at 25 °C with a dead time of 1.0 ms. The cleavage of peptides was monitored either by fluorescence of Edans peptide (ex 335 nm, em 530 nm) or by absorbance at 400 nm for pNA and pNP. Enzyme and substrates were diluted 2-fold in assay buffer. Concentrations indicated in the text of figure legends are the final concentrations after dilutions. Data were collected from the average of at least four separate measurements. The time course of fluorescence or absorbance can be described by a single-exponential equation with a steady-state term (eq 1) describe previously (24):

$$Y = B e^{-bt} + At + c \quad (1)$$

Y is the signal (fluorescence or absorbance) at time t . B is the amplitude of the burst, and b is the observed first-order rate constant governing the burst. A is the linear rate of increase in fluorescence or absorbance, and c is the background. The data were analyzed by simulation of the time courses using Pro-K global analysis/simulation program (Applied Photophysics).

pH-Rate Studies. Studies were performed on the effect of pH on both the stability of the protein and the catalytic rate. The pH stability profile of 3CL^{pro} protease was performed to ensure that velocity changes were not due to pH-dependent irreversible denaturation. A 500 nM stock of 3CL^{pro} was incubated for 10 min in 10 mM MES/BTP buffer. An overlapping buffer scheme at constant ionic strength was used to avoid buffer artifacts: MES from 5.5 to 6.5 and BTP from 6.5 to 9.5. The FRET assay with peptide 3 was used to monitor protease activity from pH 5 to 9 in 0.5 pH units. The concentrated solutions were diluted 40-fold into a 20 mM HEPES (pH 7.0) solution, and the activity was measured. In addition, the pH profile of Tamra-peptide fluorescence was performed to ensure that fluorescence did not change with pH. There was no significant difference in fluorescence of the fluorescent peptides over the pH range of 5 to 9.

The k_{cat}/K_m was measured from pH 5 to 9 in 0.5 pH increments. An overlapping buffer scheme at constant ionic strength was used to avoid buffer artifacts: 30 mM MES from 5.5 to 6.5 and 30 mM BTP from 6.5 to 9.5. Full reaction time courses were taken under pseudo-first-order conditions: 4.0 µM FRET substrate, which is much less than the K_m value. The progress curves were fit to eq 2:

$$[S] = [S_0] e^{-kt} \quad (2)$$

$[S]$ is the substrate remaining at time t , $[S_0]$ is the initial substrate concentration, and $k = (k_{cat}/K_m)[E]$. The $\log k_{cat}/K_m$ was plotted vs pH. The data were fit to eq 3 for two ionizable residues, where c is the maximum value of the k_{cat}/K_m parameter.

$$\log(y) = \log(c/(1 + [H^+]/K_a + K_b/[H^+])) \quad (3)$$

Measurement of Solvent Isotope Effects. Full progress curves were measured under first-order conditions for 3CL^{pro} in the presence of H₂O or D₂O. A 7.2% sucrose viscosity control was used to assess the impact of the more viscous D₂O ($\eta^{rel} = 1.24$). The viscosities were measured in triplicate at 21 °C with an Oswald viscometer (25). The appropriate pH meter correction was used to prepare the buffers (pD = meter reading + 0.4). The FRET assay format was modified to study the effects of D₂O on 3CL^{pro}. [²H]-HEPES and -BTP were prepared by at least three rounds of solvating HEPES and BTP in D₂O and lyophilizing the solution. 3CL^{pro} reaction solutions contained 20 mM HEPES or BTP (pH 7.0), FRET substrate, 4% DMSO, 2 mM DTT, and 0.005% Tween-20. The amount of pNA released was calculated using the molar absorptivity 13200 M⁻¹ cm⁻¹ in H₂O and 12300 M⁻¹ cm⁻¹ in D₂O. The amount of pNP released was calculated using the molar absorptivity 7160 M⁻¹ cm⁻¹ in H₂O and 4160 M⁻¹ cm⁻¹ in D₂O determined under our experimental conditions using spectrophotometric grade pNP (Aldrich Chemical Co.). The kinetic data were fit to eq 1 to obtain first-order rate constants. Division of the rate constant by the enzyme concentration resulted in k_{cat}/K_m values.

3CL^{pro} Proton Inventory Studies. Proton inventory studies were performed using either FRET (peptide 4) or colorimetric (peptide 5) assay formats. The buffer [²H]-BTP was prepared by solvating BTP in D₂O and lyophilizing the solution three times. Solutions of different H₂O/D₂O fractions (n) were prepared by mixing appropriate quantities of BTP buffers made up in H₂O and D₂O (pH 7.0, pD 6.6). Nine different values of n ranging from 0 to 1.0 were used for each substrate and six substrate concentrations were used per n value to measure the kinetic parameters.

Analysis of Proton Inventory Data. The experimental data were fit to eqs 4–6 by nonlinear regression (21, 26).

$$k_n = k_0[(1 - n + n\phi^T)/(1 - n + n\phi^G)] \quad (4)$$

$$k_n = k_0(1 - n + n\phi^T) \quad (5)$$

$$k_n = k_0/(1 - n + n\phi^G) \quad (6)$$

The reaction parameters are expressed as $k_n(n)$ functions of deuterium atom fraction n present in the isotopic solvent, where k_0 is the reaction parameter in H₂O and ϕ^T and ϕ^G are

the isotopic fraction factors of the transition-state proton and the ground-state proton, respectively.

Inactivation Studies. The inactivation of 3CL^{pro} by the Michael acceptor irreversible inhibitor PF-596162 was measured as function of time and concentration to determine the inactivation constants. Assay conditions for the inactivation of 3CL^{pro} with PF-596162 contained the following: 25 nM 3CL^{pro}, 4 μ M peptide 3, HEPES (pH 7.0), and 0.005% Tween-20. PF-596162 concentration was varied from 40 to 0 μ M with nine 2-fold dilutions. Background rates were subtracted from the rate data. The progress curves for irreversible inhibitors were fit to eq 7 where *A* equals the fluorescence of fully cleaved peptide substrate. Data was analyzed with the nonlinear regression analysis program Xlfit3.05 (ID-BS, Guildford, UK).

$$F(t) = (A)(1 - e^{-k_{\text{obs}}t}) \quad (7)$$

The k_{obs} was the pseudo-first-order rate constant for the inactivation reaction. The slope ($k_{\text{obs}}/[\text{inactivator}]$) of a plot of k_{obs} vs inactivator constant is the pseudo-second-order inhibition constant, which measures potency of the inhibitor (880 M⁻¹ s⁻¹). Alternatively, the k_{obs} was converted to $t_{1/2}$ and plotted as a function of the inverse of inhibitor concentration to yield a $K_I = 7.8 \mu\text{M}$ with a $k_{\text{inact}} = 0.012 \text{ s}^{-1}$. K_I describes the binding equilibrium, and k_{inact} describes the chemical rate of inactivation.

The pH-dependent inactivation of 3CL^{pro} (100 nM) by iodoacetamide (IA) was measured in a reaction mixture containing 20 mM BTP–MES buffer combination from pH 5 to 9 in 0.5 pH units. The FRET substrate peptide 4 was used at a 25 μM concentration with 0.001% Tween-20 and 4% DMSO. The iodoacetamide concentration was varied at 3, 1, and 0.1 mM final concentration. Inactivation progress curves were fit to eq 7 to obtain the first-order inactivation constants (k_{obs}). The second-order rate constant ($k_{\text{obs}}/[\text{IA}]$) was calculated by dividing the first-order rate constant (k_{obs}) by the concentration of iodoacetamide. Data were fit with Kaleidagraph 3.5 (Synergy Software, Reading, PA) to the equations with pH-independent rate constants and $\text{p}K_a$ values of catalytically competent functional groups. For two rate constants and two $\text{p}K_a$ values, eq 8 was used. For one rate constant and one $\text{p}K_a$ value, eq 9 was used.

$$k_{\text{obs}}/I = k_1[1/(1 + 10^{(\text{p}K_1 - \text{pH})} + 10^{(\text{pH} - \text{p}K_2)})] + k_2[1/(1 + 10^{(\text{p}K_2 - \text{pH})})] \quad (8)$$

$$k_{\text{obs}}/I = k_1[1/(1 + 10^{(\text{p}K_1 - \text{pH})})] \quad (9)$$

where k_1 and k_2 are pH-independent rate constants and $\text{p}K_1$ and $\text{p}K_2$ stand for the $\text{p}K_a$ values of the catalytically competent functional groups.

RESULTS

Enzyme Assay and Characterization. Since the foundation of meaningful mechanistic studies is based on highly purified enzyme, we sought to characterize the fraction of 3CL^{pro} that was active using an irreversible substrate mimetic (PF-596162). PF-596162 is a peptidomimetic Michael acceptor containing a weakly vinylogous ester with the following composition: 4-(2-[(4-methoxy-1*H*-indole-2-carbonyl)-amino]-

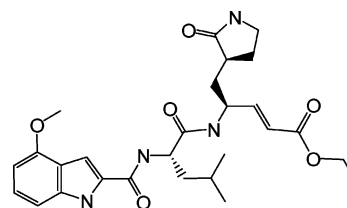


FIGURE 1: Structure of 3CL^{pro} inactivator PF-596162.

4-methyl-pentanoylamino)-5-(2-oxo-pyrrolidin-3-yl)-pent-2-enoic acid ethyl ester (Figure 1). 3CL^{pro} was inactivated by PF-596162 as described by the following kinetic parameters: $K_I = 7.8 \mu\text{M}$; $k_{\text{inact}} = 0.012 \text{ s}^{-1}$ (Figure 2A,B). Crystallographic studies have shown that the inhibitor forms a single covalent complex with the active site cysteine residue Cys145 (Jay Davies, unpublished results). A similar irreversible peptide mimetic inactivator has been shown to form a single covalent adduct with Cys145 of 3CL^{pro} (27). Isothermal titration calorimetry with PF-596162 was used to support the existence of a single binding site per monomer and to determine the fraction of the active sites occupied (Figure 2C,D). The raw titration data obtained using 60 min injection intervals was used to ensure that the irreversible covalent binding reaction was allowed to go to completion prior to making a subsequent injection (Figure 2C). The data were integrated after correcting for heats of dilution (Figure 2D). A stoichiometry of 0.96 ± 0.01 (moles of ligand per mole of 3CL^{pro} monomer equivalents) was obtained after fitting the data to a one-set-of-sites model. Calorimetry studies coupled with the pre-steady-state studies (see below) demonstrated that 3CL^{pro} was highly pure and fully active.

To measure protease activity for both amide and ester substrates, multiple assay formats (HPLC, FRET, and colorimetric) were developed. 3CL^{pro}-mediated cleavage of an untagged peptide was monitored by HPLC for the generation of two peptide products and the loss of substrate. Based on the conservation of coronavirus substrate specificities (28) and modeling studies (7), two substrates for the HPLC peptide cleavage assays (peptides 1 and 2) were designed. 3CL^{pro} cleaved peptide 1 (SITSAVLQSGFRKMA) more effectively than peptide 2 (SITSAVLQSGFRK): 45% vs 28% cleavage. Kinetic studies in the HPLC assay format were performed on the more active peptide, peptide 1, and demonstrated that it was a good substrate ($k_{\text{cat}}/K_m = 14000 \text{ M}^{-1} \text{ s}^{-1}$) (Table 1). Although the HPLC provided a direct measurement of protease activity, its throughput and sensitivity limited its utility for some mechanistic studies. A FRET assay was developed based on peptide 3, which was an amino-terminally Tamra-tagged, carboxy-terminally Dabcyl-tagged version of peptide 1. While a sensitive tool for monitoring activity, peptide 3 had low solubility (25 μM , pH 7.0), which prevented the evaluation of saturating concentrations. Pseudo-first-order conditions (4 μM peptide 3, 200 nM 3CL^{pro}) were used to assess the substrate specificity (k_{cat}/K_m) for peptide 3. The steady-state kinetic parameters are shown in Table 1. Comparison of the k_{cat}/K_m values for the untagged peptide 1 and the tagged peptide 3 demonstrated that there was minimal interference of the FRET tags at positions P₆ and P₈' on the 3CL^{pro}-mediated hydrolysis reaction. A second FRET substrate (peptide 4) was evaluated based on a previously reported 3CL^{pro} substrate (8). Peptide 4 was found to be more soluble (>100 μM at

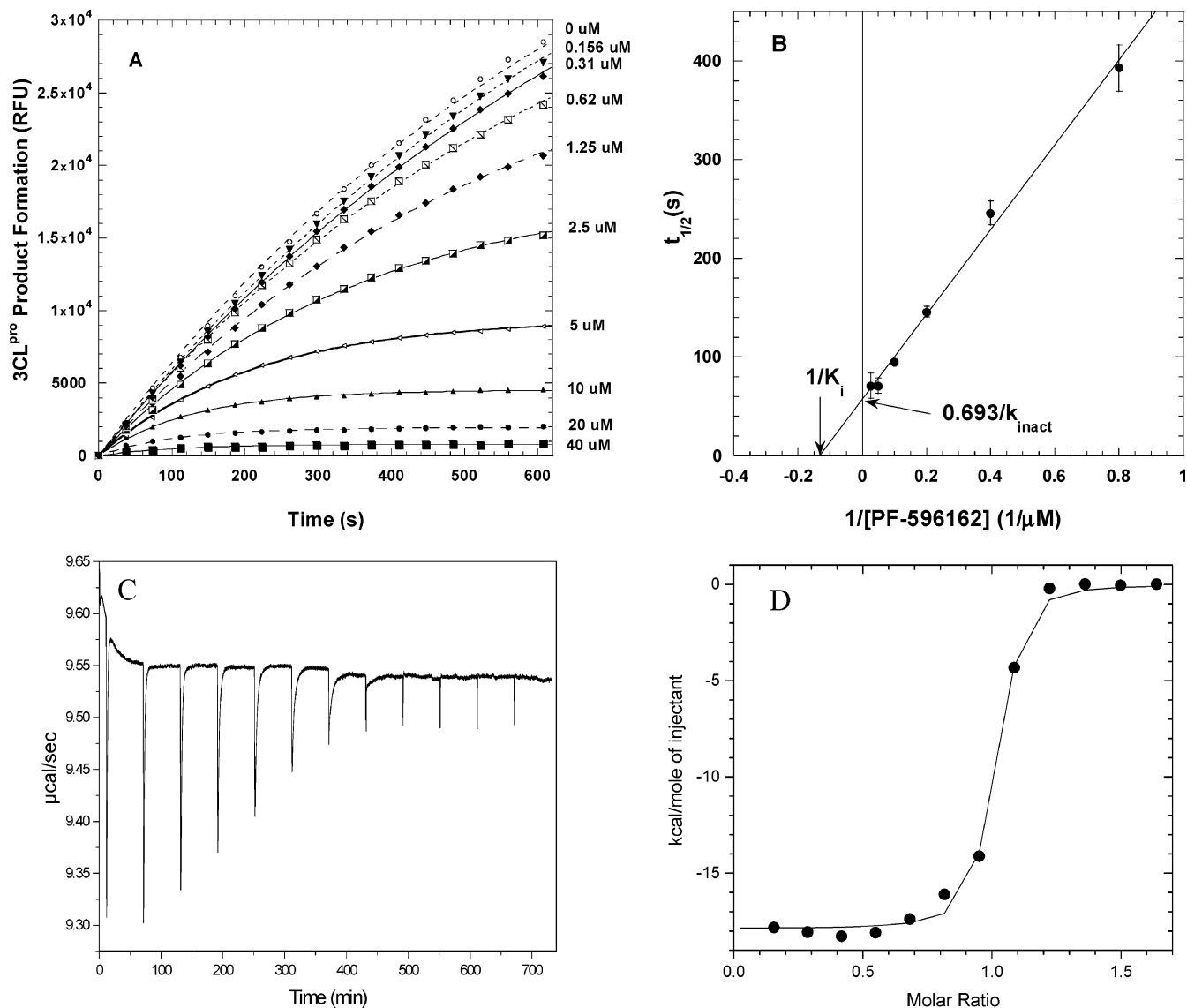


FIGURE 2: Evaluation of 3CL^{PRO} inactivator PF-596162: (A) inactivation of 25 nM 3CL^{PRO} with 4 μ M peptide 4 by titration with PF-596162; (B) plot of $t_{1/2}$ vs the inverse of the inhibitor concentration used to calculate the K_i and k_{inact} for PF-596162; (C) isothermal titration calorimetry of 186.5 μ M 3CL^{PRO} titrated into 10.0 μ M PF-596162 at 25.0 $^{\circ}$ C using 60 min injection intervals; (D) binding isotherm corrected for heats of dilution and fit to a one-set-of-sites model.

Table 1: The Steady-State Kinetic Parameters for SARS 3CL^{PRO} Peptide Substrates^a

peptide	peptidic substrates	saturation kinetics			pseudo-first-order kinetics
		k_{cat} (s^{-1})	K_m (μ M)	k_{cat}/K_m ($M^{-1} s^{-1}$)	k_{cat}/K_m ($M^{-1} s^{-1}$)
1	SITSAVLQSGFRKMA	8.5 ± 0.36	600 ± 60	14000 ± 1800	<i>b</i>
3	Tamra-SITSAVLQSGFRKMAK-Dabcyl	<i>b</i>	<i>b</i>	<i>b</i>	14000 ± 90
4	Dabcyl-KTSAVLQSGFRKME-Edans	1.5 ± 0.2	45 ± 5	34000 ± 7000	34000 ± 1500
5	SITSAVLQ-pNA (amide)	0.86 ± 0.06	180 ± 30	4800 ± 200	5000 ± 300
6	SITSAVLQ-pNP (ester)	0.60 ± 0.03	73 ± 8	8300 ± 1200	<i>b</i>

^a Peptide 1 was measured in an HPLC format. Peptides 3 and 4 were measured in a FRET format. Peptides 5 and 6 were measured in colorimetric formats. Due to poor solubility of peptide 3, k_{cat} and K_m could not be determined. There is a good correlation between the kinetic data obtained from full substrate profiles compared with that from pseudo-first-order kinetics (full progress curves). *b* Not determined.

pH 7.0) and an excellent substrate (Table 1). As measured by k_{cat}/K_m , peptide 4 was 2-fold better than peptide 1 or 3. Peptide 4 is very similar to peptide 3 with the first points of divergence from the scissile bond outward at P_7 and P_7' . A small increase in the cleavage reaction also was observed for peptide 1 compared with peptide 2, which may be due to the additional P_6' and P_7' positions. To evaluate the effect of amide hydrolysis with a good leaving group, a colorimetric

assay was developed to measure the hydrolysis of peptide 5 to release pNA. This peptide has the identical P_1 – P_8 sequence as peptides 1 and 3. With our 3CL^{PRO} protein construct, peptide 5 was a good substrate but had 3-fold less activity as measured by k_{cat}/K_m compared with peptides 1 and 3 with their natural P' amino acid sequence. Finally, to study ester hydrolysis, an assay to measure the release of pNP from peptide 6 was developed. Peptide 6 was designed

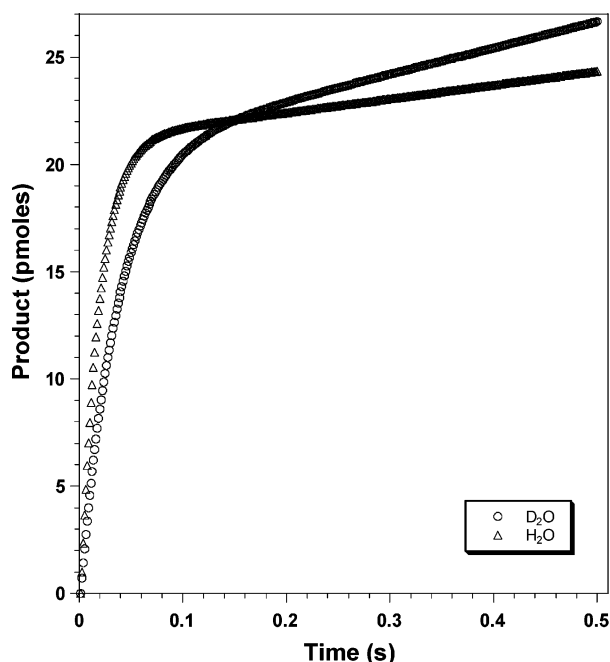


FIGURE 3: Pre-steady-state analysis of the solvent isotope effect on hydrolysis of peptide 4. The 3CL^{pro} pre-steady-state reaction time course in H₂O buffer (Δ) or D₂O buffer (\circ). Enzymatic reactions were performed in 12 mM HEPES (pH 7.0/pD 6.6 mixtures) with 1 μ M 3CL^{pro} and 12.5 μ M peptide 4.

to be identical to peptide 5 except that it had an ester as the scissile bond. The measured chemical reactivity (100 μ M peptidic substrate, pH 7.0, 22 °C) of peptide 6 to nonenzymatic hydrolysis was shown to be very large compared with peptide 5. The nonenzymatic rate of peptide 6 (5.0 pmol/s) was 3 orders of magnitude faster than that for peptide 5 (0.0026 pmol/s). Interestingly, by comparison of k_{cat}/K_m values, the ester was only a marginally better substrate compared with the highly related peptide 5 (Table 1). To confirm the kinetic findings and to provide methods amenable for additional studies, k_{cat}/K_m values were determined under pseudo-first-order conditions (Table 1). The k_{cat}/K_m values were invariant of the kinetic method used to determine them.

Pre-Steady-State Analysis. Pre-steady-state kinetic studies were initiated in order to better understand the acylation and deacylation reactions. Initial pre-steady-state studies of 3CL^{pro} showed biphasic progress curves, which are indicative of a double displacement (ping pong) mechanism (Figure 3). For our studies, we began by using a simple double displacement kinetic mechanism as a model system (Scheme 1). Pre-steady-state studies of protease-mediated ester hydrolysis by a simple double displacement mechanism described by Scheme 1 have been previously described (24). Three main parameters were obtained by pre-steady-state analysis: the burst rate (b), the burst amplitude (B), and the pre-steady-state slope (A). In the biphasic profile, b describes the rate of the initial phase, B describes the amplitude of the first phase, and A describes the rate of the second phase. The pre-steady-state slope should correspond to the steady-state rate.

Because of the high solubility of peptide 6 and its relatively low K_m value, substrate saturation of the ester substrate (peptide 6) was possible in the pre-steady-state. The pre-steady-state behavior of peptide 6 was studied at multiple

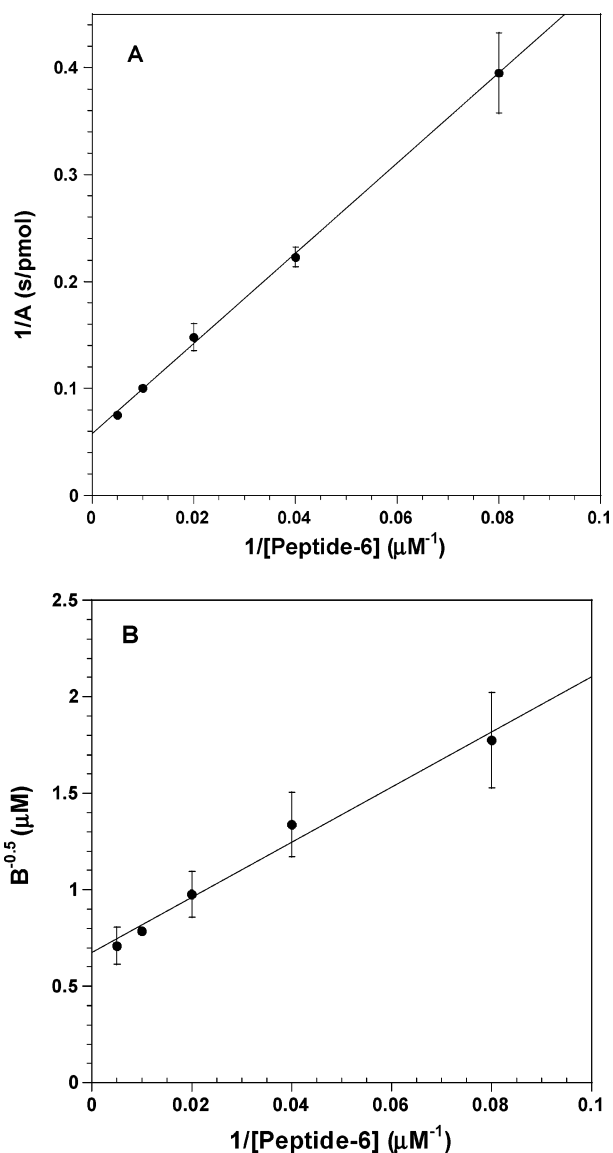


FIGURE 4: 3CL^{pro} pre-steady-state evaluation of pre-steady-state slope and burst amplitude as a function of substrate concentration: (A) reciprocal plot of the pre-steady-state slope as a function of peptide 6 concentration; (B) reciprocal plot of square root of the burst amplitude as a function of peptide 6 concentration.

concentrations (12.5, 25, 50, 100, and 200 μ M). The burst rate (b) was independent of the peptide 6 concentration, while the burst amplitude (B) and the pre-steady-state slope (A) exhibited saturation kinetics. The pre-steady-state data for burst amplitude (B) was plotted as a function of peptide 6 concentration to the following equation: $B^{-0.5} = ((k_2 + k_3)/k_2)E^{0.5} + ([K_{m,app}(k_2 + k_3)]/k_2)SE^{0.5}$ (Figure 4B) (24). The approximation of $k_2 \gg k_3$ allowed for the estimation of the enzyme concentration from the y-intercept, $2.2 \pm 0.3 \mu$ M, which matches the estimated added protein concentration (2.0 μ M). At the maximum concentration of peptide 6 (200 μ M), the burst amplitude (B) was determined to be $2.0 \pm 0.2 \mu$ M, which also supports these approximations. From the determined y-intercept and the known enzyme concentration (2 μ M), the value of $k_2/(k_2 + k_3)$ was determined to be 1.0 ± 0.1 . To achieve a value close to unity, k_2 must be much greater than k_3 . For the mechanism described in Scheme 1, the burst amplitude (B) simplifies to $B = [E]_0$ when $k_2 \gg k_3$ and $[S]_0 \gg K_{m,app}$. For 3CL^{pro}, the maximum burst amplitude

Table 2: Steady-State Analysis of the Solvent Isotope Effects on Substrate Hydrolysis^a

peptide	H ₂ O			D ₂ O			solvent isotope effect		
	k_{cat} (s ⁻¹)	K_m (μM)	k_{cat}/K_m (M ⁻¹ s ⁻¹)	k_{cat} (s ⁻¹)	K_m (μM)	k_{cat}/K_m (M ⁻¹ s ⁻¹)	$k_{\text{cat}}^{(\text{H/D})}$	$K_m^{(\text{H/D})}$	$k_{\text{cat}}/K_m^{(\text{H/D})}$
3	<i>b</i>	<i>b</i>	14000 ± 90	<i>b</i>	<i>b</i>	24000 ± 1600	<i>b</i>	<i>b</i>	0.58 ± 0.040
4	1.5 ± 0.2	45 ± 5	34000 ± 7000	3.7 ± 0.1	44 ± 7	90000 ± 11000	0.39 ± 0.05	1.0 ± 0.2	0.37 ± 0.06
5	0.86 ± 0.05	180 ± 30	4800 ± 200	0.98 ± 0.03	175 ± 16	5600 ± 200	0.88 ± 0.07	1.0 ± 0.2	0.83 ± 0.06
6	0.60 ± 0.03	73 ± 8	8300 ± 1200	0.47 ± 0.03	74 ± 7	6500 ± 1200	1.30 ± 0.14	0.99 ± 0.33	1.3 ± 0.4

^a Kinetic constants for peptides 4, 5, and 6 were measured from variable substrate concentration studies, while that for peptide 3 was measured under pseudo-first-order conditions due to insufficient solubility to achieve saturation. ^b Not determined.

Table 3: Pre-Steady-State Analysis of 3CL^{pro} Peptide Hydrolysis of Amide and Ester Substrates Including Solvent Isotope Effects^a

peptide	H ₂ O			D ₂ O			solvent isotope effect		
	B (μM)	b (s ⁻¹)	A (pmol/s)	B (μM)	b (s ⁻¹)	A (pmol/s)	B (μM)	b (s ⁻¹)	A (pmol/s)
4	0.82 ± 0.02	50 ± 2	26 ± 0.3	1.1 ± 0.06	28 ± 0.6	47 ± 0.6	0.76 ± 0.04	1.8 ± 0.1	0.55 ± 0.01
5	1.4 ± 0.3	23 ± 0.5	14 ± 1.3	1.2 ± 0.3	24 ± 2	17 ± 1	1.1 ± 0.3	1.0 ± 0.1	0.84 ± 0.07
6	1.6 ± 0.08	23 ± 0.8	10.9 ± 0.3	0.95 ± 0.11	17.2 ± 2.2	7.3 ± 0.4	0.61 ± 0.07	1.3 ± 0.2	1.5 ± 0.03

^a The amplitude of the burst (B), first-order rate of the burst (b), and steady-state rate (A) were measured. Peptide 4 was evaluated at 12.5 μM ($K_m = 44 \mu\text{M}$) with 1 μM 3CL^{pro}. Peptide 5 was evaluated at 200 μM ($K_m = 180 \mu\text{M}$) with 1 μM 3CL^{pro}. Peptide 6 was evaluated with 100 μM ($K_m = 73 \mu\text{M}$) peptide and 2 μM 3CL^{pro}.

(B) was equivalent to the amount of enzyme added. If Scheme 1 holds, this indicates that $k_2 \gg k_3$ and $[\text{S}]_0 \gg K_{m,\text{app}}$. The pre-steady-state slope data were fit to the following equation: $1/A = (1/k_{\text{cat}})E + K_{m,\text{app}}/(k_{\text{cat}}ES)$ (24) to determine $k_{\text{cat}} = 0.43 \pm 0.05 \text{ s}^{-1}$ and $K_{m,\text{app}} = 73 \pm 7 \mu\text{M}$ (Figure 4A). The k_{cat} and K_m values calculated from the evaluation of the pre-steady-state slope (A) were very similar to the values determined through steady-state analysis (Table 1). For a simple double displacement mechanism (Scheme 1), $k_{\text{cat}} = k_2k_3/(k_2 + k_3)$. If $k_2 \gg k_3$, then k_{cat} simplifies to k_3 . From the maximum pre-steady-state slope of peptide 6, we can estimate k_3 to be 0.43 s^{-1} . Finally, the burst rate data were analyzed. The burst rate $b = k_2[\text{S}]_0/(K_s + [\text{S}]_0)$ where K_s is the substrate binding constant. If $k_2 \gg k_3$, and $[\text{S}] \gg K_s$, then the burst rate (b) is equal to the acylation rate (k_2). With $K_s \gg [\text{S}]_0$, the equation simplifies to $b = k_2[\text{S}]_0/K_s$. From burst rate of peptide 6, we can estimate the lower limit of the acylation rate (k_2) to be 18 s^{-1} . The relationship $K_{m,\text{app}} = K_s k_3/(k_2 + k_3)$ has been previously described (Scheme 1) (24). With the determined value of k_2 , k_3 , and $K_{m,\text{app}}$, we can calculate the K_s to be $2900 \mu\text{M}$. K_s can be defined for Scheme 1 as $(k_{-1} + k_2)/k_1$. If there is a high commitment to catalysis ($k_2 \gg k_{-1}$), then K_s can be simplified to k_2/k_1 . With estimates of K_s and k_2 , the on-rate (k_1) can be estimated to be $6200 \text{ M}^{-1} \text{ s}^{-1}$. Another way to determine k_1 is from the k_{cat}/K_m value ($k_{\text{cat}}/K_m = k_1 k_2/(k_{-1} + k_2)$). When there is a high commitment to catalysis ($k_2 > k_{-1}$) then $k_{\text{cat}}/K_m = k_1$ (29). The steady-state k_{cat}/K_m value is similar to the k_1 determined with pre-steady-state data. This correlation indicates that the estimates of k_2 , k_3 , and K_s are reasonable. The estimate of k_1 is substantially lower than would be expected for simple diffusion-controlled binding of a substrate to an enzyme, which indicates that the process may be more complex.

With the knowledge from the evaluation of the ester substrate, peptide 6, we tried to gain mechanistic insight by studying the related amide substrates (peptides 4 and 5). Unlike the ester substrates, the amide substrates have a hydrogen bond donor in the scissile bond, which has been shown to have a significant role in catalysis for other proteases (23, 30–33). Because of insufficient solubility and higher K_m values, peptides 4 and 5 could not be saturated

under pre-steady-state experimental conditions. Nevertheless, mechanistic insight can be gleaned from the evaluation of the amide substrates (peptides 4 and 5) relative to the ester substrate (peptide 6). The three substrates were tested at K_m levels. If $k_2 \gg k_3$, and $[\text{S}] \gg K_{m,\text{app}}$, then $A = k_{\text{cat}}[\text{E}]_0$. The first condition is met ($k_2 \gg k_3$) because biphasic time-course profiles were observed for all three peptides, but the second condition was not met. The steady-state k_{cat} values can be compared with the pre-steady-state velocities by the following relationship: $A/[\text{E}]_0 = k_{\text{cat}}$ (Tables 1 and 2). The correlations between the steady-state k_{cat} values and pre-steady-state slope values were good even though the pre-steady-state substrate concentrations were at K_m levels. Because the velocity at K_m should be only 2-fold different than that at V_{max} , the similarity of the k_{cat} values derived from steady-state and pre-steady-state data is not unexpected. The amplitudes of the bursts (B) were similar to the concentration of added enzyme for peptides 4 and 5 (Table 3), even at apparently subsaturating substrate levels. The burst rate (b) of peptide 4 was 2-fold larger than that of peptide 5 or 6 (Table 3). The burst rates of peptides 5 and 6 were equivalent even though peptide 5 has an amide as the scissile bond while peptide 6 has an ester bond. Again, the enzyme-catalyzed hydrolysis of the more chemically labile ester substrate was not substantially more efficient than the corresponding amide substrates. The steady-state and pre-steady-state analysis of ester hydrolysis provided estimates of the rate constants for the individual steps of the kinetic mechanism. Pre-steady-state analysis of the amide substrates raised doubts that 3CL^{pro} has a simple double displacement kinetic mechanism because of the similarity of the ester and amide burst rates and pre-steady-state slopes.

Solvent Isotope Effect. Solvent isotope effect (SIE) studies are mechanistic tools useful in characterizing catalytically relevant proton-transfer reactions, substrate interactions, and conformational changes. SIEs probe the impact of D₂O on the enzymatic kinetic parameters. But since D₂O may have many effects (enzyme stability, conformational changes, substrate binding, and proton transfers in catalytic steps), care needs to be exercised in the interpretation of SIEs (26). For example, the higher viscosity of D₂O could affect a

physical step of the reaction. A sucrose microviscogen with the viscosity of D₂O ($\eta^{\text{rel}} = 1.24$) was determined to have no significant effect on the steady-state 3CL^{pro} reaction. Analyses of the SIEs for peptides 4, 5, and 6 were conducted in both steady-state and pre-steady-state. Normal and inverse solvent isotope effects were observed in the steady state with 3CL^{pro} (Table 2). To accurately characterize the SIEs, the SIE was determined by both pseudo-first-order conditions and a full substrate titration where possible. When pseudo-first-order conditions were used to monitor the full turnover of 1 μM peptide 4, a significant inverse SIE was observed: $k_{\text{cat}}/K_{\text{m}}(\text{H}_2\text{O}) = 34000 \pm 1500 \text{ M}^{-1} \text{ s}^{-1}$; $k_{\text{cat}}/K_{\text{m}}(\text{D}_2\text{O}) = 60000 \pm 1120 \text{ M}^{-1} \text{ s}^{-1}$; $(k_{\text{cat}}/K_{\text{m}})^{\text{H}_2\text{O}/\text{D}_2\text{O}} = 0.57 \pm 0.04$. Under similar conditions, the related peptide 3 also displayed a significant inverse SIE: peptide 3 $(k_{\text{cat}}/K_{\text{m}})^{\text{H}_2\text{O}/\text{D}_2\text{O}} = 0.58 \pm 0.04$. The enhanced solubility of peptide 4 allowed for saturation kinetics. With data from a full substrate-concentration profile, a large inverse SIE was observed for hydrolysis of peptide 4: $(k_{\text{cat}}/K_{\text{m}})^{\text{H}_2\text{O}/\text{D}_2\text{O}} = 0.37 \pm 0.06$. Peptide 5, which contained an activated amide as the scissile bond, yielded a smaller inverse SIE observed under pseudo-first-order conditions: $k_{\text{cat}}/K_{\text{m}}(\text{H}_2\text{O}) = 5000 \pm 300 \text{ M}^{-1} \text{ s}^{-1}$; $k_{\text{cat}}/K_{\text{m}}(\text{D}_2\text{O}) = 6800 \pm 200 \text{ M}^{-1} \text{ s}^{-1}$; $k_{\text{cat}}/K_{\text{m}}^{\text{H}_2\text{O}/\text{D}_2\text{O}} = 0.73 \pm 0.06$. A full substrate titration confirmed the inverse SIE: $k_{\text{cat}}/K_{\text{m}}^{\text{H}_2\text{O}/\text{D}_2\text{O}} = 0.83 \pm 0.06$ (Table 2). We determined the SIE for the ester substrate, peptide 6, which only differs from peptide 5 by having oxygen in the scissile bond. In contrast to peptide 5, there was a normal SIE observed on k_{cat} for peptide 6 (Table 2). Due to the large nonenzymatic rate for peptide 6, the analysis of the full progress curve was not attempted. Nonetheless, significant differences in the observed SIE values for ester and amide substrates were observed.

Because the 3CL^{pro} mechanism has both acylation and deacylation half-reactions, we sought to study the SIE in the pre-steady-state to characterize the acylation reaction (Table 3). Due to solubility issues encountered with pre-steady-state experimental conditions, we investigated the SIE under K_{m} conditions. The differential levels of saturation should affect the magnitudes of the effects in the pre-steady-state but not the character of the SIE (normal vs inverse). There was a large normal SIE on the burst rate of peptide 4 and an inverse SIE observed on the pre-steady-state slope (Figure 3). Peptide 5 did not have an SIE on the burst rate and had a small inverse SIE on the pre-steady-state slope. The ester substrate, peptide 6, had normal SIE values for both burst rate and pre-steady-state slope. The proton-transfer reaction of the cysteine sulfhydryl group is unique among amino acid side chains because of its low bending and stretching frequencies resulting in an inverse SIE (26, 34). The normal SIE on the burst rate is not consistent with a rate-limiting general base abstraction of a proton from the sulfhydryl group of a catalytic cysteine residue. The SIE analysis in the steady-state and pre-steady-state indicates that the 3CL^{pro} mechanism may be more complicated than the minimal protease mechanism (Scheme 1).

3CL^{pro} Proton Inventory. To gain further understanding of the underpinnings of the observed SIEs, the proton inventory technique was used to further characterize the hydrogenic sites that produced the SIEs. Proton inventories study the effect of mixtures of H₂O and D₂O on kinetic constants in the steady state (26, 34). The individual fractionation factors ϕ^{T} and ϕ^{G} measure the deuterium

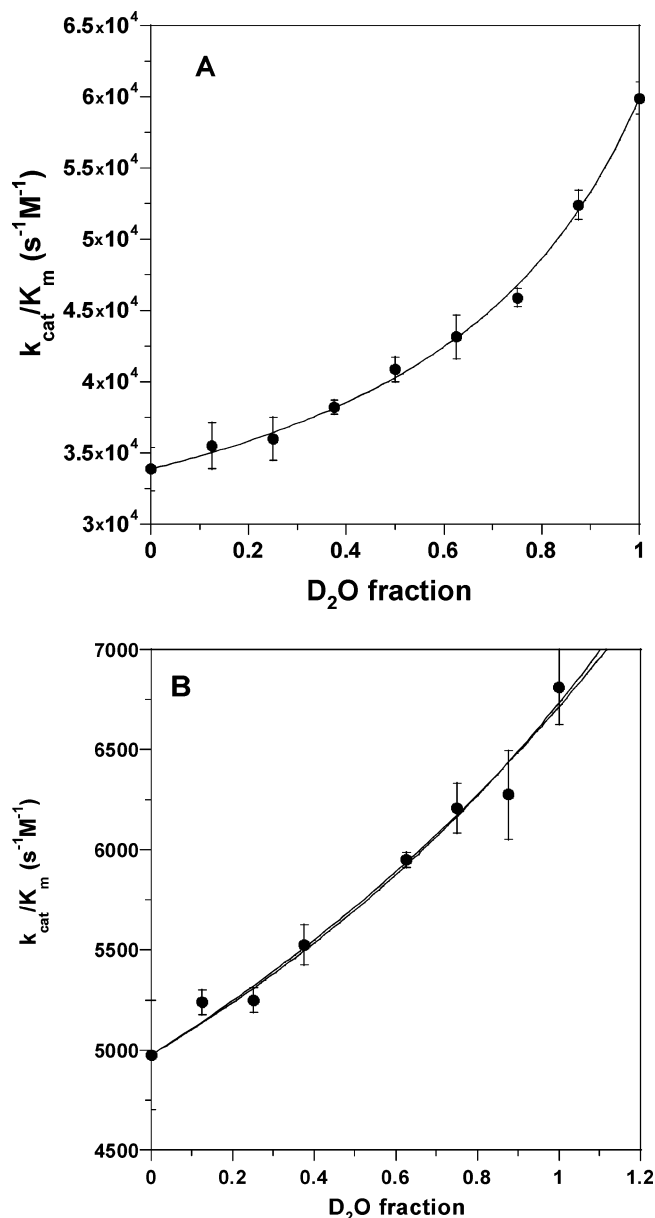


FIGURE 5: The nonlinear, least-squares fit of the $k_{\text{cat}}/K_{\text{m}}$ proton inventory data for peptides 4 and 5 (amides). Enzymatic reactions were performed in 20 mM HEPES (pH 7.0/pD 6.6 mixtures) with 400 nM 3CL^{pro} and subsaturating substrate concentrations (5 μM peptide 4 or 100 μM peptide 5): (A) data for peptide 4 was fit to eq 4, the model for two fractional factors in both the ground state and transition state; (B) data for peptide 5 with equivalent fits to the equation for fractionation factors in both the transition state and ground state (eq 4) or just the ground state (eq 6).

preference of a particular site (in the ground or transition state) relative to the deuterium preference for the bulk water (34). Bonds to neutral oxygen or nitrogen are essentially equivalent to those in bulk water and often lead to a fractionation factor of unity for ϕ^{G} . The reciprocals of the fractionation factors represent the contribution of the site to the overall solvent isotope effect. Since the observed SIEs for peptides 4 and 5 had little contribution from K_{m} , we performed a proton inventory by monitoring the full turnover of a substrate under subsaturating conditions to yield $k_{\text{cat}}/K_{\text{m}}$ values. Data for peptide 4 were fit to multiple forms of the Gross–Butler equations, eqs 4–6 (26, 34) (Figure 5A). The fit of peptide 4 data to the model with fractional factors

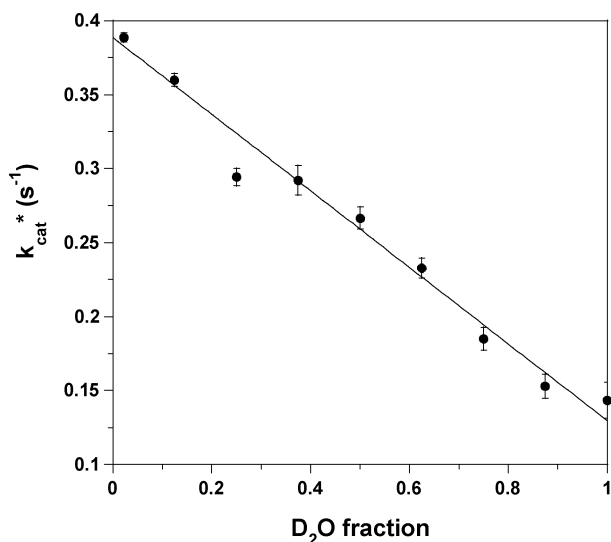


FIGURE 6: The nonlinear least-squares fit of the k_{cat} proton inventory data for peptide 6 (ester). Enzymatic reactions were performed in 10 mM HEPES (pH 7.0/pD 6.6 mixtures) with 500 nM 3CL^{pro} and a saturating substrate concentration (200 μ M peptide 6). The normal solvent isotope effect fit best to the equation for one fractionation factor in the transition state (eq 5).

in both the ground state and transition state was better (eq 4, $R^2 = 0.99$) compared with the models for a single fractionation factor in either the transition state (eq 5, $R^2 = 0.86$) or the ground state (eq 6, $R^2 = 0.95$). The fractionation factors for peptide 4 were determined to be $\phi^{\text{T}} = 0.58 \pm 0.03$ and $\phi^{\text{G}} = 0.33 \pm 0.02$. The proton inventory data for peptide 5 were fit to eqs 4–6 with equivalent fits to the equation for fractionation factors in both the transition state and ground state (eq 4, $R^2 = 0.98$) or just the ground state (eq 6, $R^2 = 0.98$) (Figure 5B). The fractionation factor for both transition state and ground state fractionation factors yielded $\phi^{\text{T}} = 0.95 \pm 0.14$ and $\phi^{\text{G}} = 0.70 \pm 0.11$, while the model for only a ground state fractionation factor yielded $\phi^{\text{G}} = 0.74 \pm 0.01$. By either fit, the contribution of ϕ^{T} to the SIE was small. With the ester substrate, peptide 6, the observed normal SIE resided in k_{cat} . Because of the significant background hydrolytic rate, the proton inventory was performed under pseudo- V_{max} conditions (500 nM 3CL^{pro}, 200 μ M peptide 6, 3 min reaction times) to obtain an estimate of k_{cat} (k_{cat}^*). This approach was facilitated by the invariance of the K_{m} as a function of D_2O content. The proton inventory for peptide 6 was fit to the equations for either one fractionation factor in the transition state (eq 5, $\phi^{\text{T}} = 0.33 \pm 0.02$, $R^2 = 0.99$) or fractionation factors in the transition state and ground state (eq 4, $\phi^{\text{T}} = 0.40 \pm 0.08$ and $\phi^{\text{G}} = 1.1 \pm 0.2$, $R^2 = 0.99$) (Figure 6). Since the ϕ^{G} is unity in the two site model, the data supports a ϕ^{T} single site model.

pH-Rate Profile. In probing the 3CL^{pro} mechanism, we sought to define the pK_{a} values of the catalytically relevant residues to see whether different substrates required different ionizable residues to affect catalysis. With a different 3CL^{pro} construct and a peptide (TSAVLQ-pNA) related to peptide 5, the pK_{a} values have been previously reported to be the following: $\text{pK}_{\text{a},1} = 6.25 \pm 0.04$ and $\text{pK}_{\text{a},2} = 8.29 \pm 0.04$ (10). Because the current studies were performed with a different, more active 3CL^{pro} construct, we sought to reinvestigate the pH-rate profile and expand the analysis to include ester hydrolysis. To ensure valid pH-rate results,

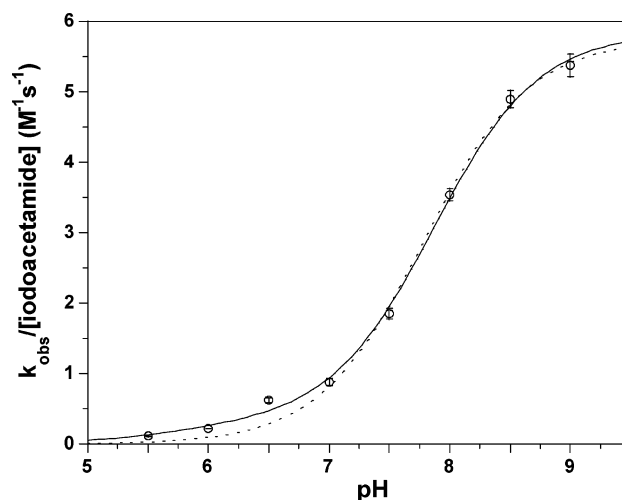


FIGURE 7: Alkylation of the catalytic cysteine with iodoacetamide. Enzymatic reactions were performed in 10 mM BTP–MES buffers (pH 5.5 to 9) with 200 nM 3CL^{pro} and 50 μ M peptide 4. Different iodoacetamide concentrations were used to measure the inactivation rates: 3 mM for pH 5.5 to 6.5, 1 mM for pH 7 to 8, and 0.1 mM for pH 8.5–9. Inactivation rates were corrected with the no iodoacetamide controls. The data fits better to an equation describing a complex ionization curve with both bell-shaped and sigmoidal terms (eq 8) (—) compared with the fit to a simple dissociation equation (eq 9) (···).

a pH-stability profile was performed on the 3CL^{pro} enzyme. 3CL^{pro} was found to be stable to irreversible pH-dependent denaturation in the examined pH range. The pH-rate behavior was then characterized for peptide 3 under pseudo-first-order conditions to determine the $k_{\text{cat}}/K_{\text{m}}$. This method of determining $k_{\text{cat}}/K_{\text{m}}$ was necessary due to solubility limitations. Fitting the data for peptide 3 to eq 3 yielded a bell-shaped profile with two pK_{a} values (6.2 ± 0.1 and 7.7 ± 0.1). The 3CL^{pro}-mediated hydrolysis of an amide substrate displayed a bell-shaped profile consistent with multiple ionizable residues contributing to catalysis.

pH-Dependent Alkylation of 3CL^{pro} with Iodoacetamide.

The profile of cysteine alkylation as a function of pH is a method to provide evidence of a thiolate–imidazolium ion pair mechanism. A thiolate–imidazolium ion pair would allow for enhanced reactivity at pH values substantially less than the pK_{a} of a typical cysteine residue. This method has been used for other cysteine proteases (18). Cysteine alkylation of 3CL^{pro} was feasible because the catalytic cysteine residue is preferentially nucleophilic. Inactivation studies with the cysteine-reactive, weakly electrophilic inactivator PF-596162 showed a 1:1 inactivation stoichiometry. Another irreversible inhibitor has been shown to specifically modify the catalytic cysteine residue of 3CL^{pro} (27). The pH dependence of the pseudo-second-order rate constant of inactivation of 3CL^{pro} ($k_{\text{obs}}/[\text{IA}]$) with iodoacetamide is shown in Figure 7. Inspection of the pH inactivation rate profile shows that it does not follow a simple dissociation curve (Figure 7). The rate of inactivation of 3CL^{pro} by iodoacetamide was significant at neutral to slightly acidic pH. The data fit better to an equation describing a complex ionization curve with both bell-shaped and sigmoidal terms (eq 8, $R^2 = 0.998$) compared with the simple dissociation curve (eq 9, $R^2 = 0.994$) (Figure 7). The fit to eq 8 resulted in the following values: $k_1 = 5.9 \pm 0.1 \text{ M}^{-1} \text{ s}^{-1}$; $k_2 = 0.29 \pm 0.18 \text{ M}^{-1} \text{ s}^{-1}$; $\text{pK}_{\text{a},1} = 5.7 \pm 0.09$; $\text{pK}_{\text{a},2} =$

7.9 ± 0.1 . The fit to eq 9 resulted in the following values: $k = 5.7 \pm 0.2 \text{ M}^{-1} \text{ s}^{-1}$; $\text{p}K_a = 7.8 \pm 0.1$. The data fits were evaluated by evaluation of the residuals (35). The residual sum of the squares for eq 8 was 0.058, while it was 0.16 for eq 9. Evaluation of the residuals to the data fits were performed by leaving one data point out and using the equations to predict the missing data. The simple model (eq 9) was less predictive at the lower pH range ($\text{pH} \leq 7$). The pH-inactivation profile (6.0 to 8.5 pH range) of PF-596162 was examined in a similar manner to iodoacetamide. PF-596162 was potent in the examined pH range with the $k_{\text{obs}}/[\text{PF-596162}]$ only reduced by 50% at pH 6.0. Although the reactivity to alkylation agents at neutral pH condition is suggestive of an active site ion-pair mechanism, it can only be considered as corroborative evidence.

DISCUSSION

Steady-State Characterization of the 3CL^{pro} Activity. The observed high enzymatic activity achieved with untagged, highly purified 3CL^{pro} was a critical prerequisite to the mechanistic analysis described in the current study. Although other laboratories have reported a similar high enzymatic activity (11, 13), there are 3CL^{pro} studies that use a construct that has 100-fold lower activity (6, 10). More recent studies have shown that extra non-native N-terminal residues have a detrimental effect on enzymatic activity (13). The catalytic activity observed for 3CL^{pro} (Table 1) are similar to or greater than the activities reported for other proteases (20, 21, 36). As such, the 3CL^{pro} preparation used in this study appears to be appropriate for meaningful mechanistic studies.

A number of studies have explored the substrate requirements of 3CL^{pro}. P4–P2' residues were reported to be indispensable for effective cleavage while P3'–P7' are not essential but have an effect on cleavage efficiency (37). An additional study of the 3CL^{pro} substrate specificity of P1–P4 substrate positions found that the P1 glutamine can be replaced by a histidine residue, the P2 leucine residue is obligate, and the P3/P4 positions are more tolerant of variation (27). Although peptides 5 and 6 have a P1' mimetic and no P2', they are good substrates. As such, the P2' position appears to be dispensable for catalysis. Peptide substrates with an amide in the scissile position (peptides 1 and 3) are cleaved 3-fold more efficiently as measured by k_{cat}/K_m compared with the peptidic substrates with an activated amide (peptide 5) or an ester substrate (peptide 6). This indicates that the leaving group may have a role in catalysis. Studies of papain by Polgar showed a substantial role of the leaving group on the substrate efficiency as measured by the k_{cat}/K_m of a large panel of substrates (33). The role of the leaving group on catalysis was fortified by using two-protonic state reactivity probes of S1–S2 to evaluate papain (32). Typically for serine/cysteine proteases, acylation is thought to be rate-limiting for amide hydrolysis while deacylation is thought to be rate-limiting for esters (18, 38). As such, enzyme-mediated hydrolysis of esters is typically faster than that with amide substrates. Analysis of 3CL^{pro} substrates demonstrated that the ester substrate peptide 6 had kinetic parameters similar to the highly related aniline substrate (peptide 5) despite the large difference in inherent reactivity. For papain, there was a large difference in k_{cat} of pNA amide substrates (X-Phe-Leu-pNA, 0.35 s^{-1}) compared with the related pNP ester substrate (X-Phe-Leu-pNP, 7.85

s^{-1}) (21). For the chymotrypsin hydrolysis of acetyl-phenylalanine substrates, the k_{cat} of the amide was 1500-fold smaller than that for the ester (38). The 3CL^{pro}-mediated hydrolysis of highly related ester and amide substrates may be distinct from chymotrypsin and papain. To further understand the ester and amide hydrolysis reactions, pre-steady-state analysis was pursued.

Pre-Steady-State Analysis. Pre-steady-state evaluation of 3CL^{pro} provided significant insight into the kinetic mechanism of 3CL^{pro}-mediated catalysis of ester and amide hydrolysis. The evaluation of ester hydrolysis as a function of substrate concentration allowed for the estimation of the rate constants of the kinetic mechanism and is consistent with a double displacement (ping pong) mechanism. Unlike related enzymes (23, 38, 39), the burst rate of 3CL^{pro}-mediated ester hydrolysis was shown to be independent of substrate concentration. The 3CL^{pro} burst rate observations can be accounted for if there was a high commitment to catalysis: the acylation rate (k_2) is much faster than the substrate dissociation rate (k_{-1}). From the burst rate of the ester substrate, we can estimate the lower limit of the acylation rate (18 s^{-1}), which was 10–100 fold higher than that for related enzymes (21). The pre-steady-state studies allowed us to estimate the substrate binding constant (K_s) and on-rate (k_1). The determined K_s and k_1 values for 3CL^{pro} were similar to values reported for related enzymes (21). The ester substrate showed that 3CL^{pro} may catalyze the acylation more effectively than papain as determined by k_1 , k_2 , and k_{-1} values. The detailed kinetic analysis of 3CL^{pro}-mediated ester hydrolysis is consistent with a kinetic mechanism similar to Scheme 1.

As observed for ester hydrolysis, the pre-steady-state progress curves for the amide hydrolysis reactions were biphasic. As expected, the 3CL^{pro}-mediated hydrolysis of amide substrates had a tight correlation between the pre-steady-state slope values and the steady-state k_{cat} values. With 3CL^{pro}, the deacylation values estimated from the pre-steady-state slopes are similar to each other: peptide 4, 1.3 s^{-1} ; peptide 5, 0.71 s^{-1} ; and peptide 6, 0.47 s^{-1} . The similarity of these values could be because the deacylation reaction occurs from a similar acyl-enzyme intermediate. But we know from SIE studies that there are significant differences in the catalytic events that govern the pre-steady-state rate. The pre-steady-state slope may include more than the deacylation reaction (P1 product release). For the serine protease chymotrypsin mediated hydrolysis of pNP esters, the burst amplitude (B) equaled the added enzyme concentration when $k_2 \gg k_3$ and $K_{\text{m,app}} \ll [\text{S}]_0$ (24). For 3CL^{pro}, the first criterion is satisfied while the second is not. Nonetheless, for peptides 4 and 5, the burst amplitude was similar to the added enzyme concentration, which again indicates an underlying mechanistic departure for the amide hydrolysis reaction.

Evaluation of the burst rate data for amide and ester hydrolysis reactions was revealing. The burst rate for peptide 4 was 2-fold faster than burst rate of the peptides with better leaving groups: pNA (peptide 5) or pNP (peptide 6). What was unexpected is that the burst rates for both peptides 5 and 6 tested at K_m levels were equivalent (Table 3). Peptides 5 and 6 form the same acyl intermediate with the scissile bond of peptide 5 being an amide while the scissile bond of peptide 6 is an ester. As such, the acylation rates are expected

to differ. If $k_2 > k_3$, then the burst rate $b = k_2[S]_0/(K_s + [S]_0)$. If $k_2 \gg k_3$ and $[S] \gg K_s$, then the burst rate (b) is equal to the acylation rate (k_2). The detailed study of pre-steady-state parameters as a function of ester concentration shows that this relationship may not hold and probably will not for peptides 4 and 5. With $K_s \gg [S]_0$, the relationship simplifies to $b = [S]_0(k_2/K_s)$. If both the amide and ester hydrolysis reactions occur with a simple kinetic mechanism (Scheme 1), then the similar burst rates should be accounted for by differing k_2/K_s ratios. To evaluate the ratio of k_2/K_s for peptides 5 and 6, one can re-evaluate the steady-state data. The steady-state K_m values for peptides 5 and 6 differ by less than 3-fold. From the relationship $K_{m,app} = K_s k_3/(k_2 + k_3)$ and $k_2 \gg k_3$, we can simplify the relationship to $K_{m,app} = K_s k_3/k_2$. Since peptides 5 and 6 form the identical acyl intermediate, the deacylation rate (k_3) by inference should be identical. The similarity of the K_m values should be propagated from the ratio of K_s/k_2 if k_3 reflects a deacylation rate. If k_2 for the ester is substantially larger than the k_2 for the corresponding amide, then the K_s must be significantly larger (poorer binding). Alternatively, the kinetic mechanism of the 3CL^{pro}-mediated amide hydrolysis may be more complicated. The rate constant k_3 for amide hydrolysis may not describe only the deacylation reaction but may encompass additional mechanistic elements (e.g., Scheme 2). His41 general-base-catalyzed hydrolysis of the highly reactive ester substrate is possible but probably unlikely due to the biphasic progress curves observed in the pre-steady state. Because the kinetic mechanism describes only the sequence of catalytic events and not the details of the catalytic mechanism, other mechanistic techniques were necessary.

3CL^{pro} Solvent Isotope Effects. Solvent isotope effect (SIE) studies of enzyme reactions provide valuable mechanistic information on proton-transfer reactions and conformational changes involved in the transition state. For typical proton-transfer reactions, an X–D bond requires more energy to break than an X–H bond and a normal SIE is observed ($\nu^{D_2O/H_2O} < 1$). A special case is the proton transfer from a sulfhydryl group in which an inverse SIE can occur ($\nu^{D_2O/H_2O} > 1$). An inverse isotope effect can be generated by events other than sulfhydryl proton-transfer reactions (e.g., conformational changes, substrate interactions). The inverse SIE on $k_{cat}/K_m^{(H_2O/D_2O)}$ previously reported for the 3CL^{pro}-catalyzed hydrolysis of the peptide substrate TSAVLQ-pNA was large (~ 0.4), but the enzyme preparation had only 1% of the enzymatic activity used in the present study (10). Since SIE determinations are sensitive to many factors, we characterized the SIE with a highly active preparation of 3CL^{pro}. In the steady state, a combination of pseudo-first-order and substrate saturation kinetic studies were used to demonstrate that there was a large inverse SIE on the 3CL^{pro}-mediated hydrolysis of the amide bonds and a normal SIE for the ester hydrolysis. The results were confirmed through the analysis of the SIE on the pre-steady-state slopes. In the pre-steady-state studies, both ester and amide substrates exhibited a normal SIE on the burst rate. This result is not consistent with a rate-limiting general base abstraction of a sulfhydryl proton. One possible explanation is that the steady-state 3CL^{pro} SIE amide results could be accounted for by an enzyme-facilitated release of the first product. Release of the amide P₁ product could be facilitated by an interaction with the NH of the leaving group or perhaps by a conformational change. Precedent for this

proposed mechanism can be found with other cysteine proteases. An interaction of backbone carbonyl of papain Asp158 with the NH of the leaving group was identified as critical for the observed inverse SIE (21, 23, 30–33). Disruption of the ion pair and formation of a new interaction of the imidazolium cation with the substrate was postulated to be responsible for the inverse SIE (20, 21). Pre-steady-state studies of the cysteine protease actinidin, but not papain, showed that a postacylation conformational change was required to release the alcohol P₁ product (23). The key residue of actinidin that influences the conformational change is Asp161, which is in an analogous position to the papain residue (Asp158) that modulates the inverse SIE (23). The difference between these residues in the pK_a was thought to be critical to their role as electrostatic modulators. For the serine protease thrombin, the inverse SIE observed is associated with a conformational change to release P₁ (40). By either mechanism, to affect P₁ release, the ester cleavage reaction cannot be facilitated by an analogous enzyme–substrate interaction. Finally, evaluation of the burst rate data provides important insight into the 3CL^{pro} mechanism. To understand the normal SIE observed on the burst rate of 3CL^{pro}, detailed studies of papain serve as a useful model to explore. Studies of papain family proteases have demonstrated that the architecture of the thiolate–imidazolium ion pair occurs at pH conditions that do not support catalysis. This led to the concept that an “electrostatic switch” modulates the thiolate–imidazolium ion pair by hydrogen-bonding interactions of an active site aspartate residue with the histidine residue of the ion pair (20, 41–43). Involvement of this interaction in the acylation reaction could lead to the observed normal SIE in the 3CL^{pro} burst. The solvent isotope studies illuminated critical similarities and differences between 3CL^{pro}-mediated ester and amide hydrolysis.

Proton Inventory. The proton inventory technique has been used to further characterize the SIE. The proton inventory describes the number of exchangeable protons in the enzyme that are involved in the catalytic mechanism resulting in the observed SIE. This technique can characterize the solvent isotope effects at each of the contributing exchangeable sites, which are quantified with fractionation factors (ϕ) (26, 34). Fractionating sites can appear in either reactant (ground) states or transition states. A ϕ value considerably smaller than unity in the transition state may be an indicator of a “proton in flight” although there are other interpretations (e.g., low-barrier hydrogen bonds). In the reactant state, there is simply a fractionating site with a stable potential. Such fractionation is expected for low-barrier hydrogen bonds, for sulfhydryl groups (where the low force constant for the S–H bond favors H over D), and for ion pairs such as thiolate–imidazolium, where a broad shallow potential (low force constant) also favors H over D. A limitation of the technique is that all solutions are not unique. For example, a linear proton inventory can be experimentally determined even though a complex array of proton-transfer reactions can occur (34). With these caveats in mind, we explored the proton inventories for both the ester and amide hydrolysis reactions. The “bowed down” shape of the proton inventory for the hydrolysis of peptide 4 by 3CL^{pro} indicates that there are two fractionating sites (exchangeable sites) involved in the acylation reaction: one in the transition state and one in the ground state. The ground-state exchangeable hydrogenic site

could be derived from the tautomerization of the reactive thiolate–imidazolium ion pair with the neutral thiol–imidazole form. The transition-state fractionation factor could be attributed to the disruption of the ion pair and the formation of a new interaction of the imidazolium cation and the substrate. A PI similar to peptide 4 was observed for papain-mediated hydrolysis of pNA peptide substrates (21). Further evidence of this mechanism for 3CL^{pro} can be garnered from the comparison of PIs with amide and activated amide substrates. The transition state has a partial bond between the catalytic cysteine residue and the substrate carbonyl carbon with the double bond character of the C=O reduced (21). The electronic nature of the carbonyl in the transition state will be affected by the leaving group. A normal amide will require more assistance than an activated amide (pNA) because the pNA can stabilize charge through resonance. The proton inventory data for peptide 5 was more consistent with a fractionating site in the ground state, while peptide 4 had fractionating sites in both the transition state and ground state. The 3CL^{pro} PI results for peptides 4 and 5 are consistent with an ion-pair mechanism for the catalysis of the acylation reaction.

From the kinetic evaluation of ester hydrolysis, we have shown that k_{cat} conditions should measure the deacylation half-reaction. The observed linear PI for 3CL^{pro} hydrolysis of peptide 6 is consistent with a single fractionating site. A possible interpretation is that His41 of the 3CL^{pro} catalytic dyad is acting as a general base to facilitate activation of water in the deacylation second half-reaction as was postulated for papain (19). Taken as a whole, the proton inventory results for the three peptides studied indicate a mechanism with the following components: (1) initiation of an ion-pair mechanism in the first half-reaction, (2) enzyme-facilitated release of the first product, and (3) general base-catalyzed deacylation reaction.

pH-Dependent Alkylation of 3CL^{pro} by Iodoacetamide. Inactivation studies with PF-596162 and studies in the literature (27) show that the 3CL^{pro} catalytic cysteine residue was preferentially nucleophilic. Inspection of the pH inactivation rate profile of iodoacetamide shows that it does not follow a simple dissociation curve (Figure 7). There is a wealth of studies of cysteine proteases that have similar pH-inactivation profiles (18). The iodoacetamide reactivity to 3CL^{pro} was significant at neutral to slightly acidic pH. A cysteine–histidine ion pair would allow for enhanced reactivity at pH values substantially less than the pK_a of an ordinary cysteine. Interestingly, the pK_a values of the ionizable residues necessary for iodoacetamide inactivation are within error of the pK_a values of catalytically relevant ionizable residues as determined from the pH–rate profiles. Although the reactivity to alkylation agents at neutral pH condition is suggestive of an active site ion-pair mechanism, it can only be considered corroborative evidence.

A Model for the Mechanism of the 3CL^{pro}. Emerging from the described studies are the details of the 3CL^{pro} kinetic steps, which can be assembled into a coherent mechanism. A key finding is that the similar 3CL^{pro} burst rates for ester and amide reactions may be attributed to a common step in the hydrolysis reactions. We propose that 3CL^{pro} may have an “electrostatic trigger” that is rate-limiting and renders the burst rate independent of substrate reactivity. Another finding is that the 3CL^{pro}-mediated ester and amide hydrolysis show

similar catalytic efficiencies while the SIE and PI studies reveal mechanistic departures. If there is an enzyme-facilitated P₁ product release due to a critical NH interaction as observed for both papain and actinidin, then only amide substrates may be able to access this mechanism. The inverse SIE and nonlinear PI results for the amide substrates are consistent with an ion-pair mechanism. Enhanced reactivity toward iodoacetamide at lower pH conditions is also indicative of an ion-pair mechanism. The normal SIE and linear proton inventory for ester hydrolysis is similar to papain and may indicate that the deacylation reaction is general base catalyzed. The proposed catalytic model for 3CL^{pro}-mediated amide hydrolysis is similar to papain, but the studied substrates indicate that it may affect catalysis differently.

ACKNOWLEDGMENT

We gratefully acknowledge Steve Grant, Karen Maegley, and Jacques Ermolieff for critically reading the manuscript and offering valued opinions. We also thank Jennifer Digits and Vladamira Heredia for technical assistance with the stopped flow experiments and Liann Wang for technical assistance with the calorimetry experiments.

REFERENCES

- Kuiken, T., Fouchier, R. A., Schutten, M., Rimmelzwaan, G. F., van Amerongen, G., van Riel, D., Laman, J. D., de Jong, T., van Doornum, G., Lim, W., Ling, A. E., Chan, P. K., Tam, J. S., Zambon, M. C., Gopal, R., Drosten, C., van der Werf, S., Escriou, N., Manuguerra, J. C., Stohr, K., Peiris, J. S., and Osterhaus, A. D. (2003) Newly discovered coronavirus as the primary cause of severe acute respiratory syndrome, *Lancet* 362, 263–270.
- Rota, P. A., Oberste, M. S., Monroe, S. S., Nix, W. A., Campagnoli, R., Icenogle, J. P., Penaranda, S., Bankamp, B., Maher, K., Chen, M. H., Tong, S., Tamin, A., Lowe, L., Frace, M., DeRisi, J. L., Chen, Q., Wang, D., Erdman, D. D., Peret, T. C., Burns, C., Ksiazek, T. G., Rollin, P. E., Sanchez, A., Liffick, S., Holloway, B., Limor, J., McCaustland, K., Olsen-Rasmussen, M., Fouchier, R., Gunther, S., Osterhaus, A. D., Drosten, C., Pallansch, M. A., Anderson, L. J., and Bellini, W. J. (2003) Characterization of a novel coronavirus associated with severe acute respiratory syndrome, *Science* 300, 1394–1399.
- Marra, M. A., Jones, S. J., Astell, C. R., Holt, R. A., Brooks-Wilson, A., Butterfield, Y. S., Khattra, J., Asano, J. K., Barber, S. A., Chan, S. Y., Cloutier, A., Coughlin, S. M., Freeman, D., Girn, N., Griffith, O. L., Leach, S. R., Mayo, M., McDonald, H., Montgomery, S. B., Pandoh, P. K., Petrescu, A. S., Robertson, A. G., Schein, J. E., Siddiqui, A., Smailus, D. E., Stott, J. M., Yang, G. S., Plummer, F., Andonov, A., Artsob, H., Bastien, N., Bernard, K., Booth, T. F., Bowness, D., Czub, M., Drebot, M., Fernando, L., Flick, R., Garbutt, M., Gray, M., Grolla, A., Jones, S., Feldmann, H., Meyers, A., Kabani, A., Li, Y., Normand, S., Stroher, U., Tipples, G. A., Tyler, S., Vogrig, R., Ward, D., Watson, B., Brunham, R. C., Krajdjen, M., Petric, M., Skowronski, D. M., Upton, C., and Roper, R. L. (2003) The genome sequence of the SARS-associated coronavirus, *Science* 300, 1399–1404.
- Eickmann, M., Becker, S., Klenk, H. D., Doerr, H. W., Stadler, K., Censini, S., Guidotti, S., Masignani, V., Scarselli, M., Mora, M., Donati, C., Han, J. H., Song, H. C., Abrignani, S., Covacci, A., and Rappuoli, R. (2003) Phylogeny of the SARS coronavirus, *Science* 302, 1504–1505.
- Sun, H., Luo, H., Yu, C., Sun, T., Chen, J., Peng, S., Qin, J., Shen, J., Yang, Y., Xie, Y., Chen, K., Wang, Y., Shen, X., and Jiang, H. (2003) Molecular cloning, expression, purification, and mass spectrometric characterization of 3C-like protease of SARS coronavirus, *Protein Expression Purif.* 32, 302–308.
- Fan, K., Wei, P., Feng, Q., Chen, S., Huang, C., Ma, L., Lai, B., Pei, J., Liu, Y., Chen, J., and Lai, L. (2004) Biosynthesis, purification, and substrate specificity of severe acute respiratory syndrome coronavirus 3C-like proteinase, *J. Biol. Chem.* 279, 1637–1642.

7. Anand, K., Ziebuhr, J., Wadhwani, P., Mesters, J. R., and Hilgenfeld, R. (2003) Coronavirus main proteinase (3CLpro) structure: Basis for design of anti-SARS drugs, *Science* **300**, 1763–1767.
8. Kuo, C. J., Chi, Y. H., Hsu, J. T., and Liang, P. H. (2004) Characterization of SARS main protease and inhibitor assay using a fluorogenic substrate, *Biochem. Biophys. Res. Commun.* **318**, 862–867.
9. Bacha, U., Barrila, J., Velazquez-Campoy, A., Leavitt, S. A., and Freire, E. (2004) Identification of novel inhibitors of the SARS coronavirus main protease 3CL(pro), *Biochemistry* **43**, 4906–4912.
10. Huang, C., Wei, P., Fan, K., Liu, Y., and Lai, L. (2004) 3C-like proteinase from SARS coronavirus catalyzes substrate hydrolysis by a general base mechanism, *Biochemistry* **43**, 4568–4574.
11. Grum-Tokars, V., Ratia, K., Begaye, A., Baker, S. C., and Mesecar, A. D. (2007) Evaluating the 3C-like protease activity of SARS-coronavirus: Recommendations for standardized assays for drug discovery, *Virus Res.*, in press.
12. Barrila, J., Bacha, U., and Freire, E. (2006) Long-range cooperative interactions modulate dimerization in SARS 3CLpro, *Biochemistry* **45**, 14908–14916.
13. Xue, X., Yang, H., Shen, W., Zhao, Q., Li, J., Yang, K., Chen, C., Jin, Y., Bartlam, M., and Rao, Z. (2007) Production of authentic SARS-CoV M(pro) with enhanced activity: application as a novel tag-cleavage endopeptidase for protein overproduction, *J. Mol. Biol.* **366**, 965–975.
14. Yang, H., Yang, M., Ding, Y., Liu, Y., Lou, Z., Zhou, Z., Sun, L., Mo, L., Ye, S., Pang, H., Gao, G. F., Anand, K., Bartlam, M., Hilgenfeld, R., and Rao, Z. (2003) The crystal structures of severe acute respiratory syndrome virus main protease and its complex with an inhibitor, *Proc. Natl. Acad. Sci. U.S.A.* **100**, 13190–13195.
15. Lee, T. W., Cherney, M. M., Huitema, C., Liu, J., James, K. E., Powers, J. C., Eltis, L. D., and James, M. N. (2005) Crystal structures of the main peptidase from the SARS coronavirus inhibited by a substrate-like aza-peptide epoxide, *J. Mol. Biol.* **353**, 1137–1151.
16. Anand, K., Palm, G. J., Mesters, J. R., Siddell, S. G., Ziebuhr, J., and Hilgenfeld, R. (2002) Structure of coronavirus main proteinase reveals combination of a chymotrypsin fold with an extra alpha-helical domain, *EMBO J.* **21**, 3213–3224.
17. Shi, J., Wei, Z., and Song, J. (2004) Dissection study on the SARS 3C-like protease reveals the critical role of the extra domain in dimerization of the enzyme: Defining the extra domain as a new target for design of highly-specific protease inhibitors, *J. Biol. Chem.* **279**, 24765–24773.
18. Brocklehurst, K., Watts, A. B., Patel, M., Verma, C., and Thomas, E. W. (1998) Cysteine Proteinases, in *Comprehensive Biological Catalysis* (Sinnott, M. L., Ed.), pp 381–423, Academic Press, London.
19. Szawelski, R. J., and Wharton, C. W. (1981) Kinetic solvent isotope effects on the deacylation of specific acyl-papains. Proton inventory studies on the papain-catalysed hydrolyses of specific ester substrates: analysis of possible transition state structures, *Biochem. J.* **199**, 681–692.
20. Theodorou, L. G., Bieth, J. G., and Papamichael, E. M. (2007) The catalytic mode of cysteine proteinases of papain (C1) family, *Bioresour. Technol.* **98**, 1931–1939.
21. Theodorou, L. G., Lympelopoulou, K., Bieth, J. G., and Papamichael, E. M. (2001) Insight into the catalysis of hydrolysis of four newly synthesized substrates by papain: a proton inventory study, *Biochemistry* **40**, 3996–4004.
22. Ferscht, A. (1999) Structure and Mechanism, in *Protein Science. A Guide to Enzyme Catalysis and Protein Folding*, (Julet, M. R., Ed.) 2nd ed., pp 472–482, W. H. Freeman and Company, New York.
23. Hussain, S., Pinitglang, S., Bailey, T. S., Reid, J. D., Noble, M. A., Resmini, M., Thomas, E. W., Greaves, R. B., Verma, C. S., and Brocklehurst, K. (2003) Variation in the pH-dependent pre-steady-state and steady-state kinetic characteristics of cysteine-proteinase mechanism: Evidence for electrostatic modulation of catalytic-site function by the neighbouring carboxylate anion, *Biochem. J.* **372**, 735–746.
24. Bender, M. L., Kezdy, F. J., and Wedler, F. C. (1967) Alpha-chymotrypsin: Enzyme concentration and kinetics, *J. Chem. Educ.* **44**, 84–88.
25. Murray, B. W., Padrique, E. S., Pinko, C., and McTigue, M. A. (2001) Mechanistic effects of autophosphorylation on receptor tyrosine kinase catalysis: enzymatic characterization of Tie2 and phospho-Tie2, *Biochemistry* **40**, 10243–10253.
26. Schowen, K. B., and Schowen, R. L. (1982) Solvent isotope effects of enzyme systems, *Methods Enzymol.* **87**, 551–606.
27. Goetz, D. H., Choe, Y., Hansell, E., Chen, Y. T., McDowell, M., Jonsson, C. B., Roush, W. R., McKerrow, J., and Craik, C. S. (2007) Substrate specificity profiling and identification of a new class of inhibitor for the major protease of the SARS coronavirus, *Biochemistry* **46**, 8744–8752.
28. Hegyi, A., and Ziebuhr, J. (2002) Conservation of substrate specificities among coronavirus main proteases, *J. Gen. Virol.* **83**, 595–599.
29. Hirohara, H., Philipp, M., and Bender, M. L. (1977) Binding rates, O–S substitution effects, and the pH dependence of chymotrypsin reactions, *Biochemistry* **16**, 1573–1580.
30. Asboth, B., and Polgar, L. (1977) Hydrolysis of alkyl ester and amide substrates by papain, *Acta Biochim. Biophys.: Acad. Sci. Hung.* **12**, 329–333.
31. Asboth, B., and Polgar, L. (1977) On the enhanced catalytic activity of papain towards amide substrates, *Acta Biochim. Biophys.: Acad. Sci. Hung.* **12**, 223–230.
32. Brocklehurst, K., Kowlessur, D., Patel, G., Templeton, W., Quigley, K., Thomas, E. W., Wharton, C. W., Willenbrock, F., and Szawelski, R. J. (1988) Consequences of molecular recognition in the S1–S2 intersubsite region of papain for catalytic-site chemistry. Change in pH-dependence characteristics and generation of an inverse solvent kinetic isotope effect by introduction of a P1–P2 amide bond into a two-protonic-state reactivity probe, *Biochem. J.* **250**, 761–772.
33. Polgar, L. (1979) Deuterium isotope effects on papain acylation. Evidence for lack of general base catalysis and for enzyme–leaving-group interaction, *Eur. J. Biochem.* **98**, 369–374.
34. Venkatasubban, K. S., and Schowen, R. L. (1984) The proton inventory technique, *CRC Crit. Rev. Biochem.* **17**, 1–44.
35. Camara, L. D., Santana, C. C., and Neto, A. J. (2007) Kinetic modeling of proteins adsorption with a methodology of error analysis, *J. Sep. Sci.* **30**, 688–692.
36. Hubbard, C. D., and Kirsch, J. F. (1968) The presteady-state kinetics of the papain-catalyzed hydrolysis of isomeric nitrophenyl esters of carbobenzoxyglycine, *Biochemistry* **7**, 2569–2573.
37. Shan, Y. F., and Xu, G. J. (2005) Study on substrate specificity at subsites for severe acute respiratory syndrome coronavirus 3CL protease, *Acta Biochim. Biophys. Sin.* **37**, 807–813.
38. Polgar, L. (1989) Serine Proteases, in *Mechanisms of protease action* (Polgar, L., Ed.), pp 87–113, CRC Press, Inc, Boca Raton, FL.
39. Wang, H., Vath, G. M., Gleason, K. J., Hanna, P. E., and Wagner, C. R. (2004) Probing the mechanism of hamster arylamine N-acetyltransferase 2 acetylation by active site modification, site-directed mutagenesis, and pre-steady state and steady state kinetic studies, *Biochemistry* **43**, 8234–8246.
40. Enyedy, E. J., and Kovach, I. M. (2004) Proton inventory studies of alpha-thrombin-catalyzed reactions of substrates with selected P and P' sites, *J. Am. Chem. Soc.* **126**, 6017–6024.
41. Menard, R., Khouri, H. E., Plouffe, C., Dupras, R., Ripoll, D., Vernet, T., Tessier, D. C., Lalberte, F., Thomas, D. Y., and Storer, A. C. (1990) A protein engineering study of the role of aspartate 158 in the catalytic mechanism of papain, *Biochemistry* **29**, 6706–6713.
42. Noble, M. A., Gul, S., Verma, C. S., and Brocklehurst, K. (2000) Ionization characteristics and chemical influences of aspartic acid residue 158 of papain and caricain determined by structure-related kinetic and computational techniques: Multiple electrostatic modulators of active-centre chemistry, *Biochem. J.* **351** (Part 3), 723–733.
43. Schlick, P., Kronovetr, J., Hampoelz, B., and Skern, T. (2002) Modulation of the electrostatic charge at the active site of foot-and-mouth-disease-virus leader proteinase, an unusual papain-like enzyme, *Biochem. J.* **363**, 493–501.